






Article

A Review of the Methods Calculating the Horizontal Displacement for Modular Reinforced Soil Retaining Walls

Xiaoguang Cai ^{1,2,3,*} , Shaoqiu Zhang ¹ , Sihan Li ^{1,2,3,*} , Honglu Xu ⁴, Xin Huang ^{1,2,3,4}  and Chen Zhu ⁵ 

¹ College of Geological Engineering, Institute of Disaster Prevention, Sanhe 065201, China; 204661132@st.cidp.edu.cn (S.Z.); huangxin2017@cidp.edu.cn (X.H.)

² Hebei Key Laboratory of Earthquake Disaster Prevention and Risk Assessment, Sanhe 065201, China

³ CEA Key Laboratory for Building Collapse Mechanism and Disaster Prevention, Sanhe 065201, China

⁴ Institute of Engineering Mechanics, China Earthquake Administration, Harbin 150080, China; xuhonglu@st.cidp.edu.cn

⁵ College of Civil and Transportation Engineering, Hebei University of Technology, Tianjin 300401, China; 194661133@st.cidp.edu.cn

* Correspondence: cxg@cidp.edu.cn (X.C.); lisihan@st.cidp.edu.cn (S.L.); Tel.: +86-15003166920 (X.C.); +86-18730659598 (S.L.)

Abstract: Most of the damage to reinforced retaining walls is caused by excessive deformation; however, there is no calculation method for deformation under static and dynamic loads in the design codes of reinforced soil retaining walls. In this paper, by collecting the measured displacement data from four actual projects, four indoor prototype tests and two indoor model tests under a total of 10 static load conditions, and comparing the calculation results with seven theoretical methods, the results show that the FHWA method is more applicable to the permanent displacement prediction of indoor prototype tests and that the CTI method is more applicable to the permanent displacement prediction of actual projects and indoor model tests. Two yield acceleration calculation methods and four permanent displacement calculation formulas were selected to calculate the displacement response of two reinforced soil test models under seismic loads and compared with the measured values, and the results showed that the Ausilio yield acceleration solution method was better. When the input peak acceleration ranges from 0.1 to 0.6 g, the Richards and Elms upper limit method is used, and when the input peak acceleration is 0.6–1.0 g, the Newmark upper limit method can predict the permanent displacement of the retaining wall more accurately.

Keywords: displacement calculation method; summary calculation; module reinforced soil retaining wall; deformation mode; yield acceleration



Citation: Cai, X.; Zhang, S.; Li, S.; Xu, H.; Huang, X.; Zhu, C. A Review of the Methods Calculating the Horizontal Displacement for Modular Reinforced Soil Retaining Walls. *Appl. Sci.* **2021**, *11*, 8681. <https://doi.org/10.3390/app11188681>

Academic Editor: Panagiotis G. Asteris

Received: 11 August 2021

Accepted: 14 September 2021

Published: 17 September 2021

Publisher's Note: MDPI stays neutral with regard to jurisdictional claims in published maps and institutional affiliations.



Copyright: © 2021 by the authors. Licensee MDPI, Basel, Switzerland. This article is an open access article distributed under the terms and conditions of the Creative Commons Attribution (CC BY) license (<https://creativecommons.org/licenses/by/4.0/>).

1. Introduction

A modular reinforced soil retaining wall is a flexible retaining structure composed of a modular panel, reinforcement, and backfill. Because of their simple structures, strong adaptability, and many other advantages, modular reinforced soil retaining walls are widely used [1–5]. However, problems related to the loss of structural function due to excessive deformation of the retaining wall have arisen in construction and use [6–8]. Robert M. Koerner et al. [6] investigated 320 damaged retaining walls, of which 99 were damaged due to excessive deformation (Figure 1). The reinforced soil retaining wall at the bridgehead approach of Xinzhuang Interchange at the turnout of Ningzhen Highway (312 National Highway)–Qixiashan Section in China [7]. In the late construction period, the southern panel of the eastern section of the bridge is obviously convex. Subsequently, due to many days of rain, the deformation of the whole wall gradually intensified, the road surface seriously subsided, and the wall was seriously tilted and bulging, which forced half of the traffic to be interrupted, and there was the possibility of collapse at any time. Hoe I. Ling et al. [8] investigated the failure of reinforced soil retaining walls in Highway 129 of

Dagong City (Figure 2) after the Chi-Chi earthquake in Taiwan in 1999 and analyzed the reasons for failure. They believed that failure was caused by the excessive displacement of the modular panel during the earthquake. The main reason for the failure of reinforced soil is that the influence of deformation on the structure is not considered in the design process.



Figure 1. Excessive deformation of the retaining wall [6].

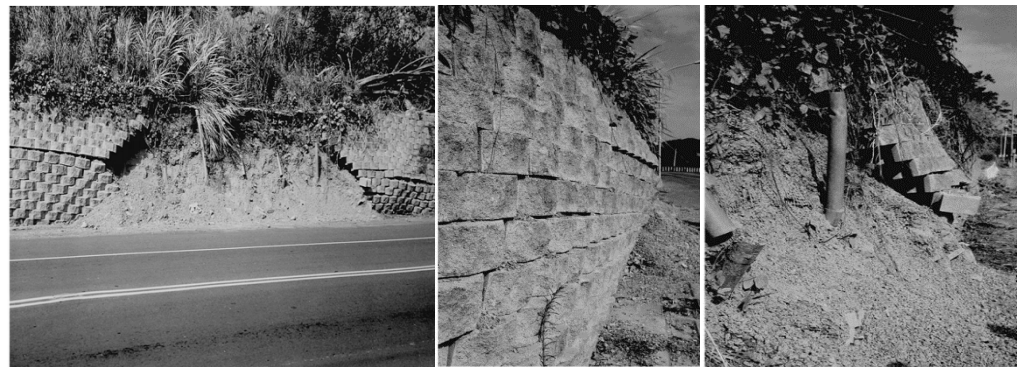


Figure 2. Failure case of reinforced soil retaining walls under earthquake action [8].

At present, the steps for the design of modular reinforced soil retaining walls are as follows (based on the [9,10] railway subgrade retaining structure design specification, 2006): (1) determine the engineering conditions. (2) Determine the engineering parameters. (3) Determine the wall height, wall panel and reinforcement parameters. (4) Check the external stability. (5) When the internal stability is checked, there is no deformation checking process or steps. Because the panel, reinforcement, backfill, and foundation conditions will lead to and affect the deformation, it is very important to find a reliable deformation calculation method. Many scholars have performed relevant research on deformation calculations.

For the method for calculating the deformation of reinforced soil retaining walls under static forces, Wang et al. [11] calculated the equivalent reinforced soil retaining wall structure for horizontal isotropic vertical elastic beams, according to Rayleigh-Ritz method, and the calculation method of horizontal displacement of reinforced soil retaining wall under static force was deduced, while the deformation was the sum of the bending deformation and shear deformation.

Mahsa Khosrojerdi et al. [12] introduced six calculation methods for the horizontal deformation of reinforced soil retaining walls and reinforced abutments (FHWA method, GeoService method, CTI method, JeWell-Miigan method, Wu method, and Adams method). Among them, the FHWA method is an analysis formula based on the regression analysis of actual engineering and numerical simulation results, and the maximum horizontal deformation can be calculated only by the reinforcement length (L) and retaining wall height (H). The GeoService method is based on the limit equilibrium theory. The horizontal deformation of each layer can be calculated only by knowing the limit strain or the maximum strain and length of each layer. Based on actual engineering and finite element analysis, the CTI

method for calculating the structural deformation during the service period can be used to calculate the horizontal deformation of each layer if the ultimate strain or the maximum strain of each layer of the reinforcement and the height of the retaining wall are required. The Wu method is based on the lifting method of the Jewell and Milligan method, which can be used to calculate the horizontal deformation of each layer without considering the strain of the reinforcement and the influence of the panel stiffness. The Adams method assumes that the volume strain is 0, the synchronous deformation of the reinforcement and soil, and the horizontal strain is less than 1%, which can be used to calculate the horizontal deformation of the top of the structure.

Mahsa Khosrojerdi et al. [12] compared the six methods with the experimental data of 17 reinforced soil retaining walls and reinforced abutments to determine the practicability of the six calculation methods. Krystyna Kazimierowicz-Frankowska [13] reviewed five calculation methods for the deformation of reinforced soil retaining walls, and the advantages and disadvantages of these five calculation methods were explained. At the same time, an IBWPAN method that can evaluate strain-displacement was introduced. The IBWPAN method divides the displacement into the creep displacement of the free zone and the tensile displacement of the anchorage zone, and the horizontal displacement calculation is divided into three modes: (1) the mode where only the displacement generated by the free zone is calculated; (2) the mode without external loads, the displacement of the free zone and the anchorage zone; and (3) the mode with external loads, the displacement of the free zone and the anchorage zone. He [14] established a numerical model through FLAC^{3D}, summarized the horizontal deformation formula of reinforced soil retaining walls, and obtained the formula of each influencing factor and the horizontal deformation of retaining walls, as well as the horizontal deformation formula of reinforced soil retaining walls containing each influencing factor. Each calculation method is summarized in Table S1.

For the deformation of reinforced soil retaining walls under seismic loads, Z. Cai and R.J. Bathurst [15] compared several calculation methods (Newmark upper bound method, Richards and Elms upper bound method, Whitman and Liao average fitting method, and Cai and Bathurst method) and showed that although different methods are calculated with different parameters, the permanent displacement values obtained by all methods are in a reasonable area. Budhu [16] used the sliding safety factor method to analyze the yield acceleration of a backpacked reinforced soil retaining wall. Younan et al. [17] simplified the retaining wall as a cantilever spring model and proposed a calculation method of the retaining wall deformation considering panel stiffness. Based on the calculation method of horizontal displacement of reinforced soil retaining walls under static action, Wang et al. [11] deduced the theoretical research formula for the horizontal seismic deformation of reinforced soil retaining walls under seismic action by using the quasi-static method. After analyzing the existing models (Ambraseys and Menu method, Jibson method, and Roberto method), Xu et al. [18] established a permanent displacement prediction model based on the critical acceleration ratio, Arias strength, and seismic residual strength by using a large number of strong motion records recorded during the Wenchuan earthquake. The energy method was used to convert the measured displacement of the slope into the permanent displacement of the slope without a supporting structure, and the validity of the model was verified by the measured data.

Although there are many calculation methods under static load and seismic load, there is no recognized calculation method because of the accuracy of the data. Dunncliff [19] judged the reliability of measured data by numerical calculation, and Pantelidis [20] compared solutions, design specifications and centrifuge tests to support the effectiveness of the proposed coefficients. In order to find a suitable deformation calculation method for modular reinforced earth retaining wall, this paper first describes the actual deformation of retaining wall under 10 static loads, and predicts the displacement by seven calculation methods. Then, through two indoor dynamic test models, the measured displacement values are compared with the calculated values under four calculation methods to verify the

accuracy of the calculation method. Finally, the calculation method that is most suitable for predicting displacement under static and dynamic loads is obtained. The research results can provide reference for the deformation design of modular reinforced earth retaining wall.

2. Study on the Deformation under Static Forces

2.1. Study on the Deformation Mode

Many experts and scholars have performed relevant research on the deformation mode of modular reinforced soil retaining walls under static action (Figure 3), which is mainly divided into tilting types (Figure 3a) and bulging types (Figure 3b).

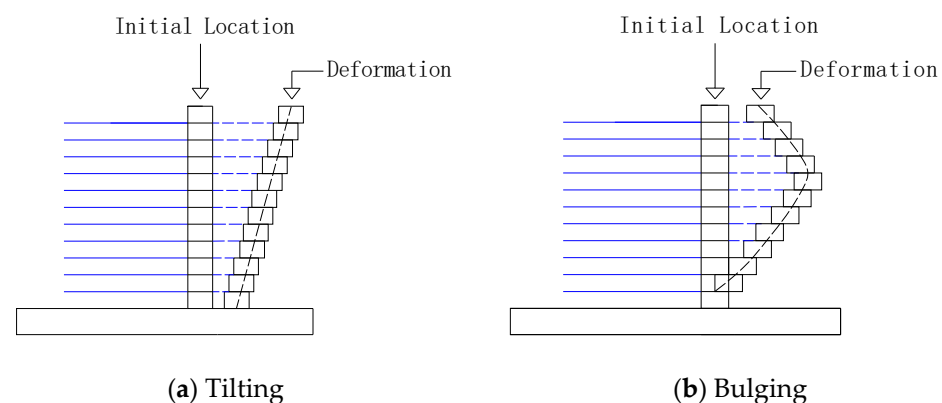


Figure 3. Horizontal deformation mode of the reinforced soil retaining wall.

Bathurst et al. [21] introduced deformation monitoring of a 6.1 m-high modular reinforced soil retaining wall in Illinois, USA, after completion and after loading. The monitoring results are shown in Table 1.

Table 1. Deformation after completion and loading.

Condition	Wall Surface			Inside a Soil-Mass		
	Maximum Deformation Position	Maximum Deflection	Deformation Mode	Maximum Deformation Position	Maximum Deflection	Deformation Mode
107 days after completion	3.07 m	19.56 mm	Bulging	6.1 m	28.7 mm	Tilting
370 days after loading	3.07 m	91.44 mm	Tilting	6.1 m	60.71 mm	Tilting

N. Abu-Hejleh et al. [22] introduced the deformation response of reinforced soil retaining wall abutment structures completed near Denver, Colorado, in 1999 during the construction period. The maximum outward displacements of Section 200, Section 400, and Section 800 are 7, 9 mm and 10 mm, respectively. Among them, the maximum deformation positions of Section 200 and Section 800 are equal to 2/3 of the wall height, and the deformation mode is bulging. The maximum deformation position of Section 400 is at the top of the wall, and the deformation mode is an outward-dip type. This may be due to the difference in the deformation modes caused by different construction seasons and different construction processes.

Hatami et al. [23,24] and Bathurst et al. [25,26] introduced four 3.6 m high reinforced soil retaining walls constructed by the Royal Canadian Military Academy, and four models were different due to different spacings and stiffnesses of the reinforcement. In the observation after completion and after loading, the maximum deformation position is approximately 2.7 m high, and the deformation mode bulges.

Jennifer E. Nicks et al. [27] developed a model with dimension of 1.4 m (length) \times 1.4 m (width) \times 2.0 m (height) to study the deformation mode of reinforced soil columns.

The deformation modes under different loads, different ultimate tensile forces of the reinforcement, and different vertical spacings were obtained. The test results show that the maximum lateral deformation occurs at a height of one-third from the top regardless of whether the veneer is included in the test process, and the overall deformation trend is inclined.

Xiao et al. [28] made a retaining wall with dimensions of 1.0 m (length) \times 0.54 m (height) to analyze the influence of the distance between the strip foundation and wall panel on the deformation characteristics of the reinforced retaining wall. The results show that when the foundation deviation distance D is less than $0.5 H$, the top deformation of the retaining wall is the largest, and the overall deformation trend is inclined. When D is $0.6H$ and $0.8H$, the deformation of the upper part of the retaining wall is the largest, and the overall trend changes to bulging.

In conclusion, due to different factors, such as the height of the retaining wall, the length of the reinforcement, the spacing of the reinforcement, the stiffness of the reinforcement, the construction season and the construction sequence, the modular reinforced soil retaining wall has different deformation modes and deformation amounts. Therefore, it is necessary to evaluate the applicability and accuracy of existing deformation calculation methods.

2.2. Comparison of the Measured Data and Calculation Methods

To analyze the applicability of the deformation calculation methods, this paper uses the measured values of 10 modular reinforced soil retaining walls to calculate the results of the FHWA (F) method, GeoService (G) method, CTI (C) method, Wu (1,2) method, Adams (A) method, and Wang (W) method, and analyzes the practicability of seven calculation methods. Table S2 summarizes the parameters of the 10 structures. Models 1, 2, 3, and 4 are practical engineering, models 5, 6, 7, and 8 are indoor prototype tests (1:1 indoor model test is carried out according to the test prototype), and models 9 and 10 are indoor model tests (according to the test prototype, the indoor model test designed by similarity ratio).

Table S3 lists the measured values of 10 cases and the calculated values of 7 calculation methods under static P (kPa). Figures 4–6 show the comparison between the calculated values and the measured values (M) under each working condition. Because the calculated results of the IBW PAN method and He Wei method are negative and inconsistent with the actual situation, they are not included in the table. In this paper, the η value (1-calculated value/measured value) is defined. When η is 0, the predicted value is the same as the measured deformation. When the η value is greater than 0, the prediction method is not conservative, and the prediction method with an η value less than 0 represents the conservative prediction method. In 10 cases η the values are shown in Table 2 and Figure 5. The displacement value of case 9 under FHWA method in Figure 5 is -466.71 , which is excessively conservative, so it is not shown in Figure 5.

Table 2. η value.

	F	G	C	Wu(1)	Wu(2)	A	W
1	−0.30	0.58	0.06	−	−	−	−
2	−	−2.00	−0.53	−2.25	−	0.18	−
3	−	−0.38	0.08	−0.50	−	−0.58	−
4	−	−0.80	−0.20	−0.95	−	−0.58	−
5	−2.51	0.60	0.22	0.67	0.96	−3.11	−4.01
6	−0.89	0.79	0.58	0.82	0.92	−3.11	−4.01
7	−7.13	−1.08	−3.08	−0.73	1.00	−3.11	−4.01
8	−2.72	0.58	0.17	0.61	0.88	−3.11	−4.02
9	−466.71	0.33	−0.81	−	−	−0.8	−
10	−11.56	0.75	0.51	0.02	−	−	−

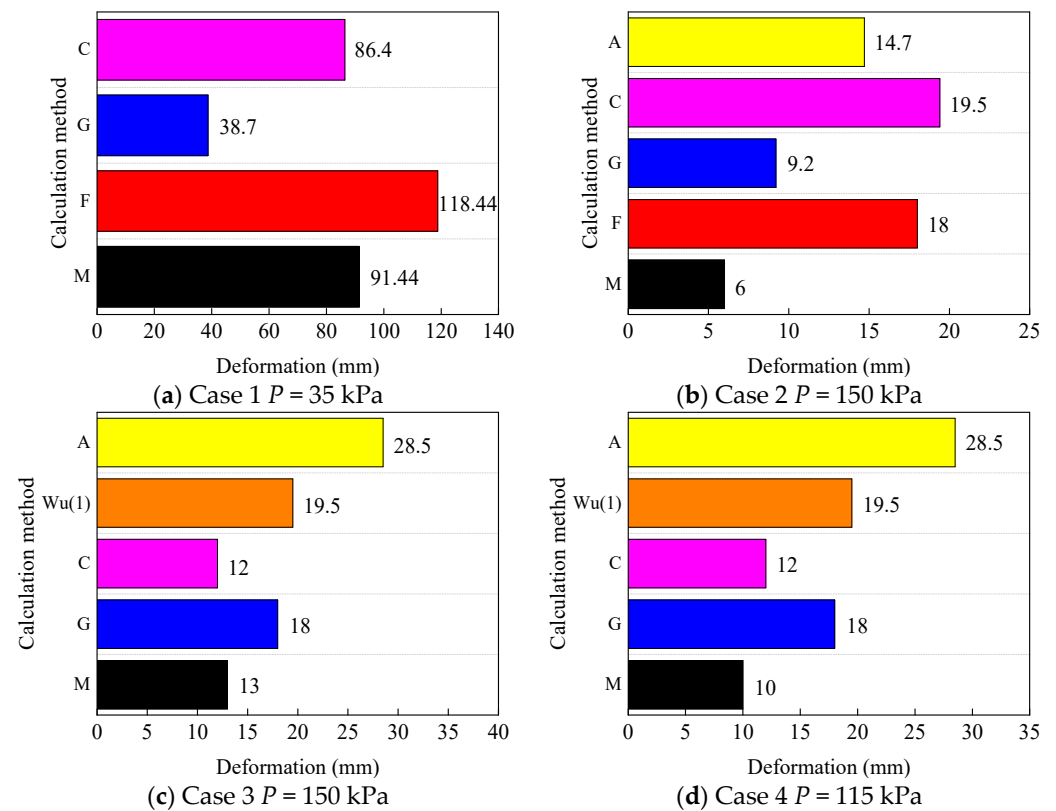


Figure 4. Comparison between measured value and calculated value in case 1–4.

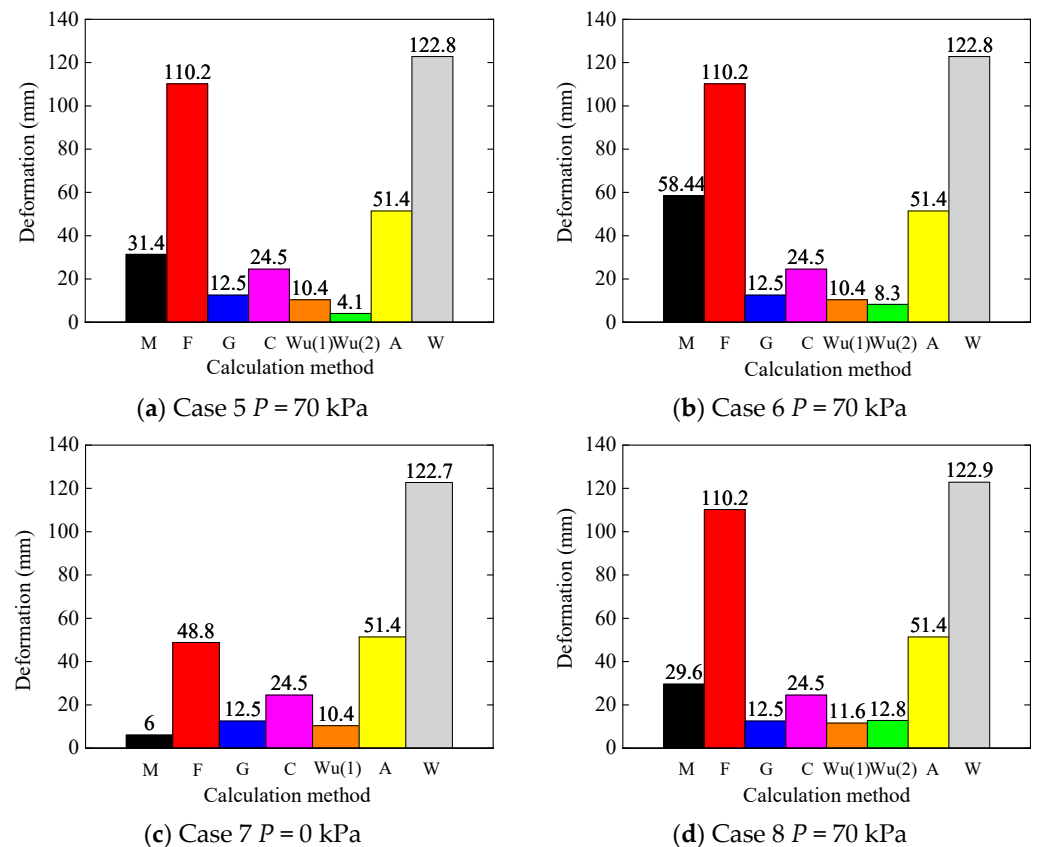


Figure 5. Comparison between measured value and calculated value in case 5–8.

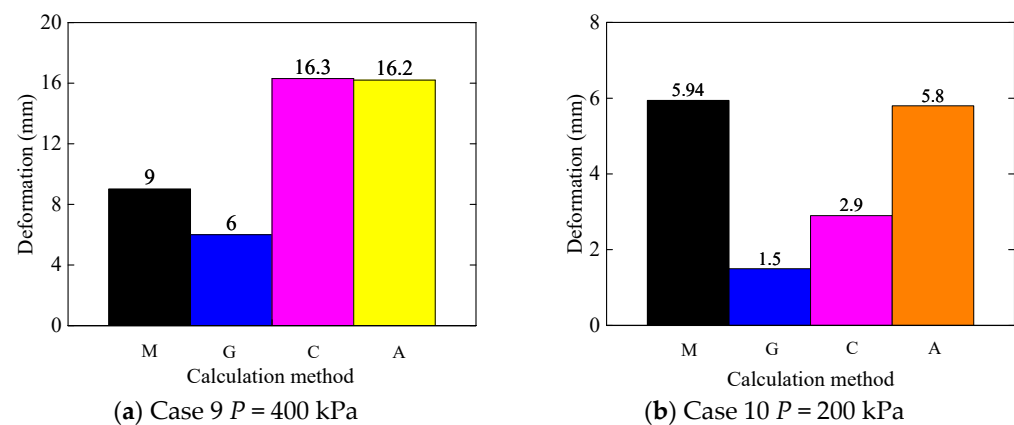


Figure 6. Comparison between measured value and calculated value in cases 9–10 (note: since the calculated values under the FHWA method in case 9 and case 10 are 4209.4 and 74.6, respectively, which are excessively conservative, they are not shown in the figure.).

The seven calculation methods are not applicable to all cases, and there may not be parameters in the formula in the case. The L/H values of case 2–4 under FHWA method are 1.778–2.667, 1.355–2.033, 1.355–2.033, respectively, which are not between 0.3 and 1.175, which do not meet the conditions of formula, so the permanent displacement value cannot be obtained. In case 1 of the Wu (1) method, the reinforcement stiffness (K) parameter is missing. Case 9 cannot get a displacement because $L/H = 0.5$ is less than 0.7. In cases 1–4 and 10 under Wu (2) method, due to the lack of the friction angle (δ) between the module bricks and the friction angle between the brick and soil (β), in case 9, since L/h is 0.5 less than 0.7, the displacement value cannot be obtained. Due to the lack of data in case 1 and case 10 under the Adams method, the displacement value cannot be obtained. Under the W method, case 1 lacks the geogrid elastic modulus (E_r) geogrid Poisson's ratio (ν_r), cases 2–4 lack the geogrid elastic modulus (E_r) and the fill elastic modulus (E_s), and case 9 and case 10 lack the fill elastic modulus (E_s), so the calculated value cannot be obtained.

As can be seen from Figure 7, the calculation results under seven calculation methods, η_n value analysis shows that, in 10 cases, the relative difference between the CTI method and the GeoService method is the smallest, because most η_n value is less than 0, so the existing calculation methods are conservative in predicting deformation, and the FHWA method is the most conservative. In cases 1–4 of the practical engineering cases, the GeoService method and CTI method show good practicability. Although the two methods need accurate reinforcement strain in calculation, the CTI method has less difference, so the CTI method is more accurate in displacement prediction in practical engineering. In cases 5–8 of the indoor prototype test, the relative difference between the Adams method and the Wang (W) method is the largest, so both methods are not suitable for the prediction of indoor prototype test displacement, while the CTI method, GeoService method, and Wu (1) method show good practicability. In case 7, the GeoService method is more conservative than the Wu (1) method; therefore, the Wu (1) method is more appropriate. In cases 9–10, the relative differences obtained by GeoService method, CTI method, and Wu (1) method are similar. Therefore, the GeoService method and CTI method have shown good performance in predicting indoor model tests. Comparing the calculated/measured values of the GeoService method and the CTI method, the ratios of the two calculation methods are 1.5, 3.96, 0.55, and 2.048, respectively, in cases 9 and 10. Because the difference between the calculated value and the measured value of CTI method is smaller, the CTI method is selected as the displacement prediction method of the indoor model test. The GeoService method and CTI method can get the predicted value when predicting 10 cases, so they are more practical than the other five methods.

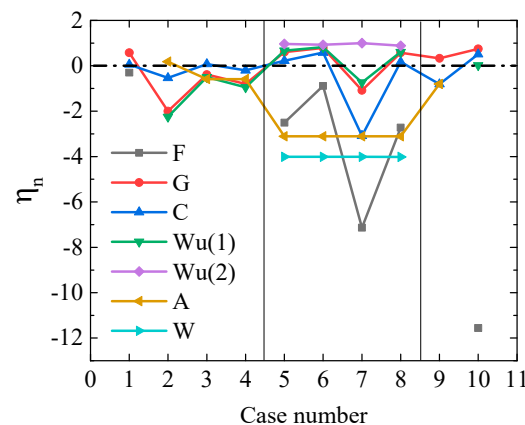


Figure 7. η_n value analysis diagram.

2.3. Discussion

The model fabrication process in the model test and indoor prototype test is rigorous and precise, so the deformation is small. The construction quality of actual projects is often difficult to guarantee due to factors such as the construction period and cost. Robert M. Korrner et al. [6] considered that improper filler, poor compaction effect, unreasonable design, and poor drainage were the main reasons for the failure of 320 reinforced soil retaining walls. At the same time, because the modulus of the foundation soil, the stiffness of the reinforcement, the vertical spacing of the reinforcement, the length of the reinforcement, the nature of the backfill soil, the change in the wall height, the additional load, the depth of the panel foundation and other factors will affect the deformation of the reinforced soil retaining wall, it can be speculated that an accurate deformation calculation method does not exist.

According to the suggestion of the η value, the FHWA method is used to predict the deformation value before the construction of a modular reinforced soil retaining wall. Under the premise of known reinforcement deformation, the Wu (1) method and CTI method are used to estimate the deformation of modular reinforced soil retaining walls in normal use.

3. Study on the Deformation under Seismic Loads

3.1. Calculation Method of the Yield Acceleration

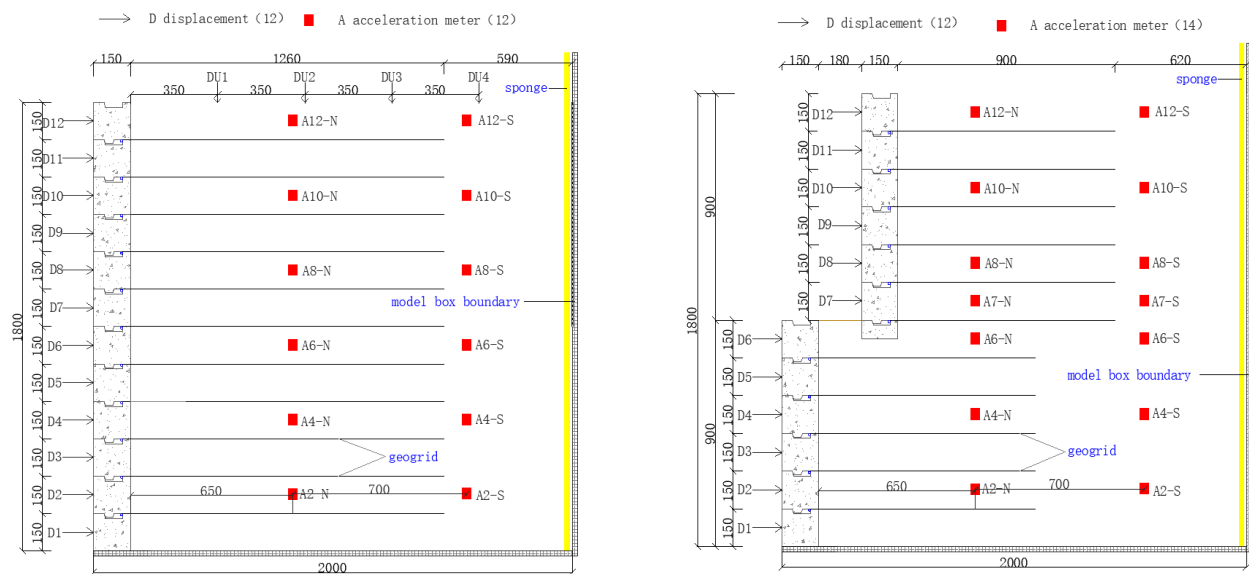
Under seismic loading, the displacement calculation of reinforced soil retaining walls is generally based on the Newmark sliding block method. The Newmark sliding method theory was originally used to estimate the permanent displacement of embankment slope caused by earthquake. When the ground acceleration exceeds the critical acceleration of the soil, the block will move. Other calculation methods are modified and improved on the basis of the Newmark method. For example, Whitman and Liao carried out regression analysis on Newmark displacement data and put forward formulas for estimating permanent displacement.

The test data selected Li et al.'s [29] single-step, two-tiered modular reinforced soil retaining wall model scale test, and the test parameters are shown in Table 3. The model size of the single-step modular reinforced soil retaining wall is $2.0 \times 1.5 \times 1.8$ m (length \times width \times height), which is divided into 12 layers, and the height of each layer is 0.15 m. To monitor the displacement response of the retaining wall under input acceleration, a rod displacement meter is arranged at the middle position of each layer module, for a total of 12 displacement meters, and an accelerometer is arranged from the bottom to the top of each pair of layers in the reinforced area and non-reinforced area, for a total of 12 locations, to obtain the acceleration response. The size of the two-tiered modular reinforced soil retaining wall model and the layout of the accelerometer and the top rod displacement

meter are the same as those of the single-step modular reinforced soil retaining wall model. The design diagram of the two models is shown in Figure 8.

Table 3. Calculation and test parameters.

Model Types	Angle of Internal Friction $\varphi/^\circ$	Reinforcement Spacing b/m	Reinforcement Length L/m	Height of the Retaining Wall H/m	Inclined Angle of the Wall Back $\beta/^\circ$
Single-step block	41	0.15	1.26	1.8	0
Two-tiered block	41	0.15	0.9	1.8	0



(a) Single-step modular reinforced retaining wall. **(b)** Two-tiered modular reinforced retaining wall.

Figure 8. Model plane diagram.

The yield acceleration method proposed by Newmark gives the acceleration value when the safety factor is 1. When the yield acceleration value is greater than the input acceleration value, displacement accumulation will occur. By summarizing and analyzing the results of previous studies and large shaking table tests, Muni obtained the yield acceleration formula through the safety factor of anti-slip earthquakes. E. Ausilio applied the limit analysis method to obtain the yield acceleration method under seismic loads. Table 4 introduces four calculation methods for the yield acceleration. The calculated values of the yield acceleration of reinforced retaining walls with two different forms of panels under the Muni method and E. Ausilio method are shown in Table S4.

Table 4. Calculation value of the yield acceleration.

Serial Number	Calculation Method	Single-Step Block	Two-Tiered Block
1	Muni Budhu method [16]	0.34 g	0.32
2	E. Ausilio method [30]	0.36 g	0.36

3.2. Calculation Method of the Permanent Displacement

The empirical formula method is one of the main contents of the residual displacement estimation method of reinforced soil retaining walls after earthquakes. Table S5 summarizes five empirical formula methods, namely, the Richards method [31], Whitman method [32], Cai and Bathurst method [15], and Newmark method [33]. The five methods are based on the critical acceleration coefficient k_c , peak acceleration k_m and propagation velocity V_m of seismic waves. The V_m values of the two shaking table tests are shown in Table 5.

Table 5. Peak velocity values of the reinforced soil retaining wall of the single-step module and two-tiered module V_m (m/s).

Peak Acceleration (g)	Single-Step Block				Two-Tiered Block	
	Ratio of Similitude 1:2		Ratio of Similitude 1:4		Ratio of Similitude 1:10	
	WL wave	EL wave	WL wave	EL wave	WL wave	EL wave
0.1	0.06	0.07	0.04	0.05	-	-
0.2	0.07	0.11	0.06	0.08	0.07	0.1
0.4	0.09	0.17	0.1	0.13	0.13	0.17
0.6	0.12	0.2	0.1	0.15	-	-
0.8	0.16	0.26	0.13	0.2	0.26	0.3
1	0.2	0.32	0.15	0.24	-	-

3.3. Comparison between the Experimental and Calculated Values

By analyzing the η_n values of two different panel forms of modular reinforced soil retaining walls under the action of WL waves and EL waves, the practicability of four calculation methods for the displacement prediction of modular reinforced soil retaining walls is judged. The meaning of η_n is shown in Table 6.

Table 6. Description of the method.

η_n	Implication
η_1	1 – Richard method calculated value/measured value
η_2	1 – Cai method calculated value/measured value
η_3	1 – Whitman method calculated value/measured value
η_4	1 – Newmark method calculated value/measured value

3.3.1. Comparative Analysis of the Test Values and Measurement Values of the Single-Step Module Shaking Table

The η_n obtained by the four calculation methods in Figures 9 and 10 show that with the increase of input ground motion, the relative difference under each calculation method increases gradually, indicating that the deviation between the calculated value and the measured value is getting larger and larger, and the difference between each method is increasing. When the η_n value was at the initial 0.1 g, each η_n value was the closest. With the increase of acceleration, the gap between each η_1 , η_2 and η_3 , η_4 values showed an increasing trend, and the size and trend of η_1 and η_2 were almost consistent from beginning to end. When the similarity ratio is 1:4, the WL wave is input. When the peak acceleration is less than 0.6 g, the η_n values are all greater than 0, and the calculated values are less than the measured values. When the peak acceleration reaches 1.0 g, the η_n values are all less than 0, and the calculated values are greater than the measured values. The calculated values are conservative. When the peak acceleration is 0.1–0.6 g, the η_1 values are smaller than other η_n values, which can be predicted by the Richards and Elms upper bound method. When the peak acceleration is 0.6–1.0 g, the $\eta_1 < \eta_2 < \eta_4 < \eta_3$; that is, the Richards and Elms upper bound method < Cai and Bathurst average upper bound method < Newmark upper bound method < Whitman and Liao average fitting method. Correspondingly, EL wave is input at the similarity ratio of 1:2. When the input peak acceleration is 0.1–0.6 g, η_n values are greater than 0, η_1 values and η_2 values are close to 0, and when the input peak acceleration is 0.8–1.0 g, η_n values are all less than 0, η_3 and η_4 are much larger than η_1 and η_2 . At this time, η_3 minimum distance from 0 line, and the Whitman and Liao average fitting method is more suitable for predicting the displacement value. Comparing Figures 8 and 9, it can be seen that the η_n value under the Ausilio calculation method is generally closer to the 0 value line than that under the Muni method, so the Ausilio method is more suitable.

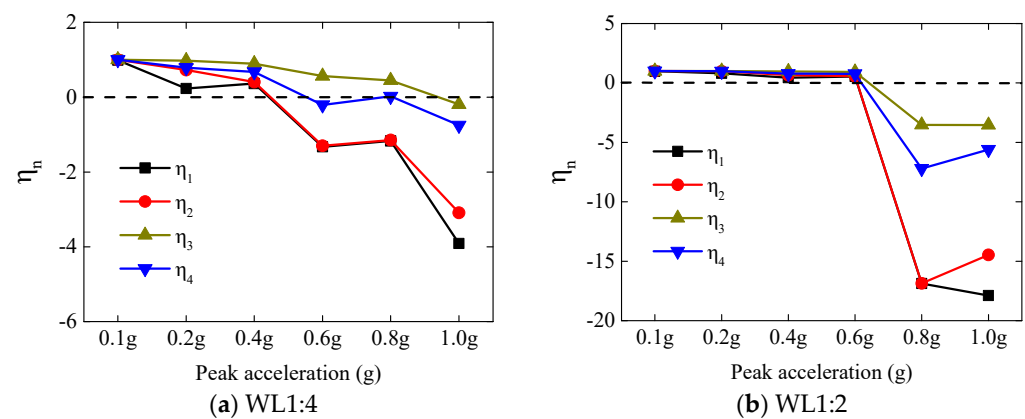


Figure 9. Muni method [16] under WL wave η_n value.

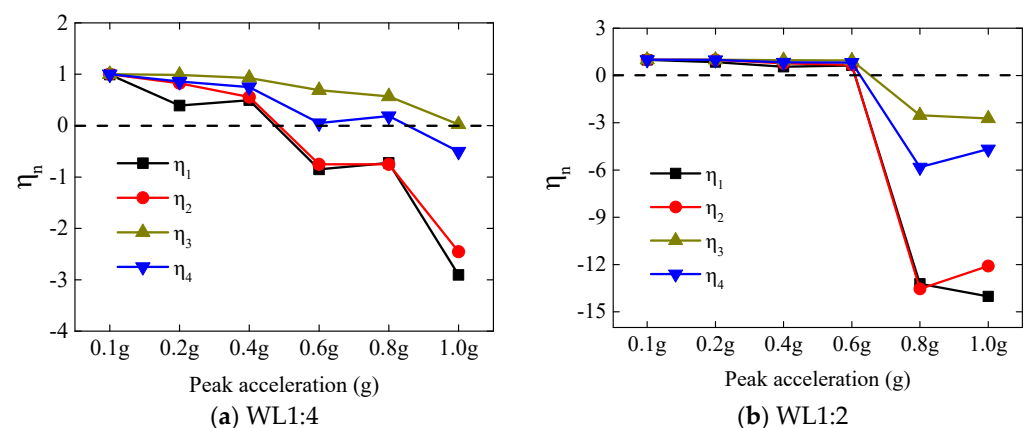


Figure 10. Ausilio [31] method under the WL wave with the η_n value.

Figures 11 and 12 show that the value of η_n decreases with the increase of input peak acceleration, and the change amplitude is larger and larger. Under the condition of similarity ratio 1:4 and similarity ratio 1:2, the change trend of η_n value is consistent. With the increase of peak acceleration, the trend line of η_1 value and η_2 value is gradually away from η_3 and η_4 . At 1.0 g, η_1 and η_2 are farthest from η_3 and η_4 . In the case of similarity ratio 1:4, when the input peak acceleration is 0.1–0.6 g, the η_1 value is less than 0 under 0.2 g in Figure 11, and the other values are greater than 0, which shows that each calculation method is conservative in predicting the displacement value under small earthquakes, and the η_1 value is relatively more reasonable, so Richards and Elms upper bound method is more reasonable. When the input peak acceleration is 0.8–1.0 g, the η_1 and η_2 values are gradually away from the zero line, so Richards and Elms upper bound method and Cai and Bathurst average upper bound method are not applicable at this time. Relatively speaking, η_3 and η_4 values show good applicability, η_4 value is more conservative, so the Whitman and Liao average fitting method is more reasonable. When the similarity ratio is 1:2, the input peak acceleration is 0.1–1.0 g, and the η_n value gradually decreases. When the similarity ratio is 0.1–0.4 g, the η_n values are all greater than 0, and the η_1 value is smaller. Therefore, the Richards and Elms upper bound method is suitable for this stage. At 0.6–1.0 g, the η_4 value is more conservative than the η_3 value, and the Whitman and Liao average fitting method is more suitable.

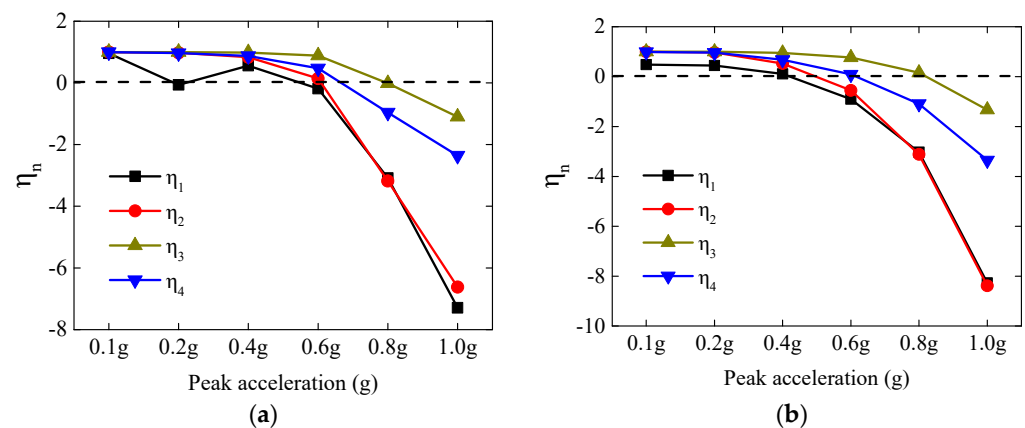


Figure 11. Under the yield acceleration obtained by the Muni method [16] under the EL wave and η_n value.

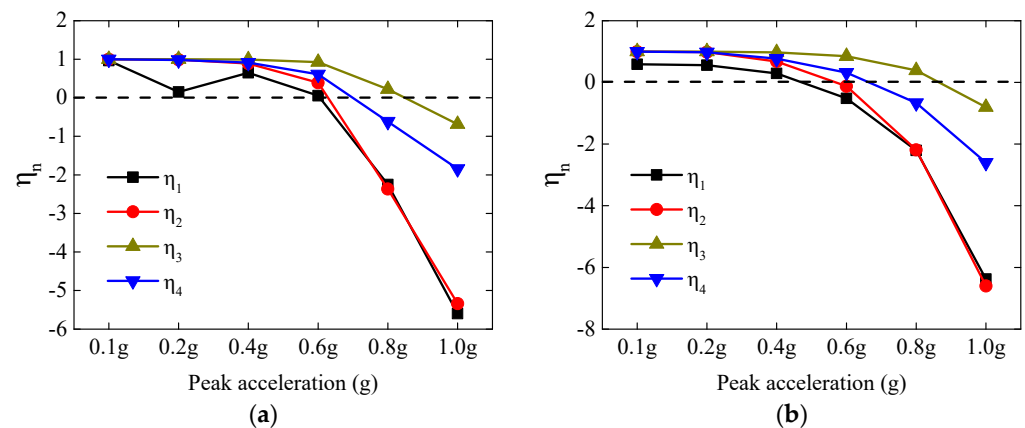


Figure 12. Ausilio [31] method under the EL wave and η_n value.

3.3.2. Comparative Analysis of the Test and Measurement Values of the Two-Tiered Module Shaking Table

Figures 13 and 14 show that the change trend of the two-tiered modular reinforced earth retaining wall under earthquake is the same as that of the single-step modular reinforced earth retaining wall. When the input peak acceleration is small, the value of η_n is greater than 0. With the increase of the peak acceleration, the value of η_n decreases gradually. When the input peak acceleration is 0.2–0.4 g, Richards and Elms upper bound method can better predict the displacement value. When the similarity ratio is 1:10, the Cai and Bathurst average upper bound method is more suitable for the input of WL wave. When EL wave is input, Whitman and Liao average fitting method and Newmark upper bound method are both suitable. Since η_4 is more conservative, the Whitman and Liao average fitting method is selected. The η_n values of yield acceleration obtained by the Ausilio method were 0.76372, −0.14144, −9.89728 and −56.87885 under the EL wave at 0.2–1.2 g, respectively. The η_n values of yield acceleration obtained by Muni method were 0.7029, −0.43424, −12.69613, and −10.83064. At this time, the calculated value obtained by the Ausilio method is closer to the measured value. Thus, the Ausilio method is more accurate than the Muni method.

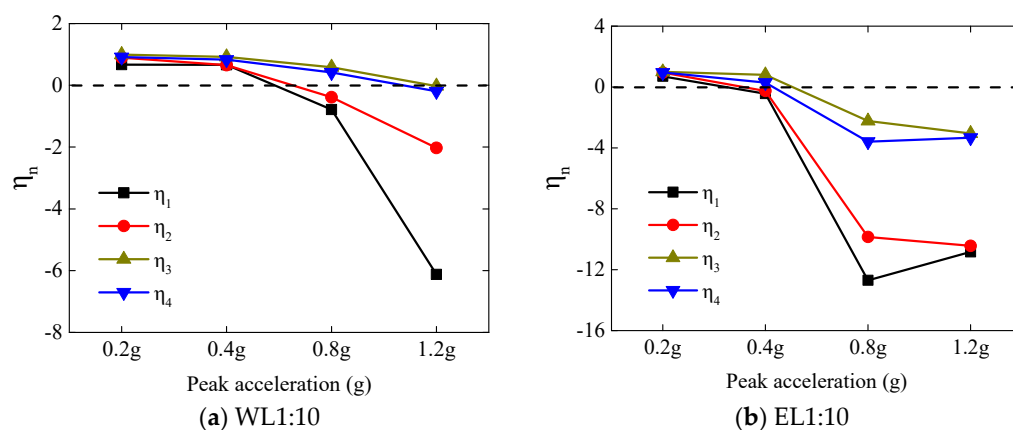


Figure 13. Muni method [16] for yield acceleration at a value of η_n .

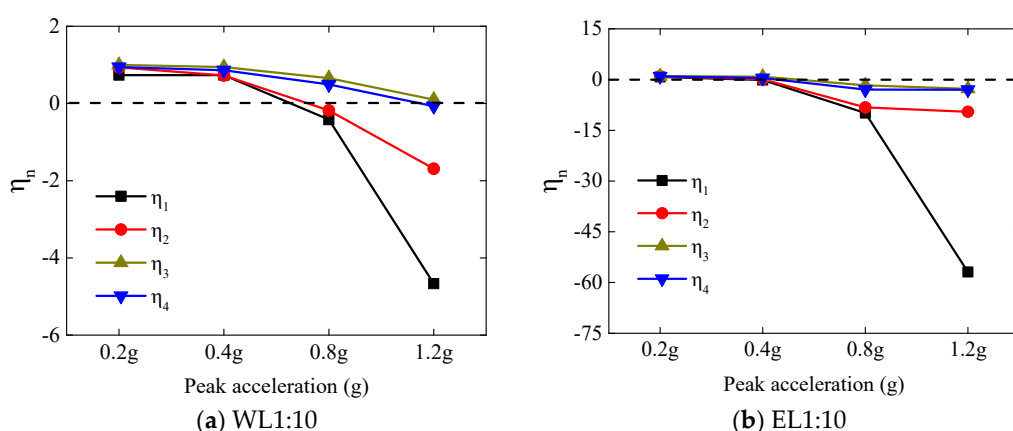


Figure 14. Ausilio method [31] used to calculate the yield acceleration at a value of η_n .

3.4. Discussion

According to the Newmark sliding block method theory, the reason for the accumulation of permanent displacement after an earthquake is that when the input peak acceleration k_m is greater than the critical acceleration k_c , there is no displacement when k_c is less than k_m . In the actual process, when k_c is less than k_m , there is still a gradual decrease in the internal soil; that is, there will be a small displacement. Therefore, although the yield accelerations calculated by the Muni method and E. Ausilio method are greater than the peak acceleration of the partial input, various calculation methods can be used to predict the generation of the displacement.

In the single-step and two-tiered reinforced soil retaining wall models, the η_n values obtained under the yield acceleration values obtained by the E. Ausilio method and the Muni method are compared. The η_n value under the E. Ausilio method is smaller than that under the Muni method, and the measured value is closer to the calculated value. Therefore, the E. Ausilio method is more suitable for the displacement prediction of modular reinforced soil retaining walls. The E. Ausilio method is more suitable because the yield acceleration obtained by this method is slightly larger than Muni method, so the displacement value is more accurate.

4. Conclusions

In this paper, the experimental and calculated values are compared, and the calculation methods suitable for predicting the behavior of modular reinforced soil retaining walls under static and dynamic loads are obtained, and suggestions are provided for future experimental analysis and practical engineering.

(1) In the prediction of retaining wall calculation method under static action (P), since the FHWA method only requires few parameters (wall height and reinforcement

length), the deformation value can be roughly estimated before the construction of modular reinforced retaining wall; the FHWA method is the most conservative method and the Wu (1) method is the least conservative method. Under the premise of knowing the deformation of reinforcement, the GeoService method is an accurate method to predict the lateral deformation. It is more practical to select the CTI method without knowing the strain of reinforcement. Therefore, the CTI method is recommended to estimate the normal deformation of modular reinforced earth retaining wall.

(2) By comparing the η_n values of single-step and two-tiered modular reinforced earth retaining walls, it can be seen that the η_n values are quite different when the peak acceleration is less than or greater than 0.6 g, which also leads to the need to use different calculation methods to predict the results. When the input peak acceleration is 0.1–0.6 g, the actual displacement value can be calculated by the Richards and Elms upper bound method through numerical calculation. When the input peak acceleration is 0.6–1.0 g, the Whitman and Liao average fitting method can truly reflect the permanent displacement of the retaining wall.

(3) Since the measured values of permanent displacement of modular reinforced earth retaining wall under static and dynamic actions are relatively large, the panel is prone to damage. Therefore, engineers should evaluate the displacement in the early and after the actual construction, and take the horizontal displacement as one of the indicators to evaluate the safety of the project.

Supplementary Materials: The following are available online at <https://www.mdpi.com/article/10.3390/app11188681/s1>, Table S1: Calculation methods of the deformation of RSRW under static loading, Table S2: Reinforced soil retaining wall parameters of 10 case histories, Table S3: Measured and predicted maximum lateral deformations of GRS walls, Table S4: Introduction of the yield acceleration, Table S5: Calculation method of the horizontal displacement for the retaining wall under earthquake action. Reference [34] refer to the supplementary material.

Author Contributions: Conceptualization, S.Z.; methodology, S.L.; validation, H.X.; formal analysis, X.H.; data curation, C.Z.; writing—original draft preparation, X.C. All authors have read and agreed to the published version of the manuscript.

Funding: The research reported in this manuscript was supported by the Earthquake Technology Spark Program of China (no. XH204402); the Fundamental Research Funds for the Central Universities (no. ZY20215107); and the National Natural Science Foundation of China (no. 51778144).

Institutional Review Board Statement: Not applicable.

Informed Consent Statement: Not applicable.

Data Availability Statement: This study did not report any data.

Acknowledgments: The writers appreciate the assistance provided by Li Zhang, BaoShuang Jin, and Guanhao Shen when discussing the analytical methods.

Conflicts of Interest: The authors declare no conflict of interest.

References

1. Yoo, C.; Jung, H.Y. Case history of geosynthetic reinforced segmental retaining wall failure. *J. Geotech. Geoenviron.* **2006**, *132*, 1538–1548. [\[CrossRef\]](#)
2. Allen, T.M.; Bathurst, R.J. Design and performance of 6.3m high, block-faced geogrid wall designed using k-stiffness method. *J. Geotech. Geoenviron.* **2013**, *140*, 13–16.
3. Allen, T.M.; Bathurst, R.J. Performance of an 11m high block-faced geogrid wall designed using k-stiffness method. *Can. Geotech. J.* **2013**, *51*, 16–29. [\[CrossRef\]](#)
4. Riccio, M.; Ehrlich, M.; Dias, D. Field monitoring and analyses of the response of a block-faced geogrid wall using Dine-grained tropical soils. *Geotext. Geomembr.* **2014**, *42*, 127–138. [\[CrossRef\]](#)
5. Wu, L.; Yang, G.; Zhang, Q.; Sun, H.; Zhang, L.; Jiao, R.; Qian, S. In-situ test on dynamic responses of reinforced soil retaining walls for high-speed railways. *J. Southwest Jiaotong Univ.* **2017**, *52*, 546–553.
6. Koerner, R.M.; Koerner, G.R. An extended data base and recommendations regarding 320 failed geosynthetic reinforced mechanically stabilized earth (MSE) walls. *Geotext. Geomembr.* **2018**, *46*, 904–912. [\[CrossRef\]](#)

7. Zhang, B.; Shi, M.; Bai, S. Research on failure of xinzhuang clay-reinforced soil wall. *Rock Soil Mech.* **2007**, *28*, 2348–2352.
8. Hoe, I.L.; Dov, L.; Nelson, N.S.C. Post-earthquake investigation on several geosynthetic-reinforced soil retaining walls and slopes during the Ji-Ji Earthquake of Taiwan. *Soil Dyn. Earthq. Eng.* **2001**, *21*, 297–313.
9. FHWA-NHI-10-024. *Design and Construction of Mechanically Stabilized Earth Walls and Reinforced Soil Slopes—Volume I*; U.S. Department of Transportation Federal Highway Administration: Washington, DC, USA, 2009.
10. Industrial Standard of the People's Republic of China TB10025-2006. *Code for Design of Railway Subgrade Retaining Structures*; China Railway Press: Beijing, China, 2006.
11. Wang, L.; Chen, G.; Jing Lai, S. Pseudo-static method for horizontal deformation of geo-grid reinforced soil retaining wall under earthquake. *China J. Highw. Transp.* **2015**, *28*, 28–34.
12. Khosrojerdi, M.; Xiao, M.; Qiu, T.; Nicks, J. Evaluation of prediction methods for lateral deformation of GRS walls and abutments. *J. Geotech. Geoenviron. Eng.* **2017**, *143*, 06016022. [[CrossRef](#)]
13. Kazimierowicz-Frankowska, K. Deformations of reinforced-soil retaining walls. In Proceedings of the 11th International Conference on Geosynthetics, Seoul, Korea, 16–21 September 2018.
14. He, W. *Study on Deformation of Reinforced Retaining Wall*; Chongqing Jiaotong University: Chongqing, China, 2016.
15. Cai, Z.; Bathurst, R.J. Deterministic sliding block methods for estimating seismic displacements of earth structures. *Soil Dyn. Earthq. Eng.* **1996**, *15*, 255–268. [[CrossRef](#)]
16. Ramakrishnan, S.; Budhu, M.; Britto, A. Laboratory seismic tests of geotextile wrap-faced and geotextile-reinforced segmental retaining walls. *Geosynth. Int.* **1998**, *15*, 255–268. [[CrossRef](#)]
17. Younan, A.H.; Veletos, A.S. Dynamic response of flexible retaining walls. *Earthq. Eng. Struct. D.* **2000**, *29*, 1815–1844. [[CrossRef](#)]
18. Xu, G.; Yao, L.; Li, C.; Wang, X. Predictive models for permanent displacement of slope based on recorded strong-motion data of wenchuan earthquake. *China J. Geotech. Eng.* **2012**, *34*, 1131–1136.
19. Pantelidis, L. The Generalized Coefficients of Earth Pressure: A Unified Approach. *Appl. Sci.* **2019**, *9*, 5291. [[CrossRef](#)]
20. Dunncliff, J. *Geotechnical Instrumentation for Monitoring Field Performance*; John Wiley & Sons: New York, NY, USA, 1993; ISBN 0471005460.
21. Bathurst, R.J.; Simac, M.R.; Christopher, B.R.; onczkiewicz, C.B. A database of results from a geosynthetic reinforced modular block soil retaining wall. In Proceedings of the Full Scale Experiments of the 80's, ISSMEE/ENPC, Paris, France, 18–19 November 1993; pp. 341–365.
22. Abu-Hejleh, N.; Zornberg, J.G.; Wang, T.; Watcharamonthein, J. Monitored Displacements of unique geosynthetic-reinforced soil bridge abutments. *Geosynth. Int.* **2002**, *9*, 71–95. [[CrossRef](#)]
23. Hatami, K.; Bathurst, R.J. Development and verification of a numerical model for the analysis of geosynthetic-reinforced soil segmental walls under working stress conditions. *Can. Geotech. J.* **2005**, *42*, 1066–1085. [[CrossRef](#)]
24. Hatami, K.; Bathurst, R.J. Numerical model for reinforced soil segmental walls under surcharge loading. *J. Geotech. Geoenviron.* **2006**, *132*, 673–684. [[CrossRef](#)]
25. Bathurst, R.J.; Vlachopoulos, N.; Walters, D.L.; Burgers, P.G.; Allen, T.M. The Influence of facing stiffness on the performance of two geosynthetic reinforced soil retaining walls. *Can. Geotech. J.* **2006**, *43*, 1225–1237. [[CrossRef](#)]
26. Bathurst, R.J.; Nernheim, A.; Walters, D.L.; Allen, T.M.; Burgess, P.; Saunders, D.D. Influence of reinforcement stiffness and compaction on the performance of four geosynthetic-reinforced soil walls. *Geosynth. Int.* **2009**, *16*, 43–56. [[CrossRef](#)]
27. Nicks, J.E.; Esmaili, D.; Adams, M.T. Deformations of geosynthetic reinforced soil under bridge service loads. *Geotext. Geomembr.* **2016**, *44*, 641–653. [[CrossRef](#)]
28. Xiao, C.; Chen, Q.; Han, J.; Chen, P. Experimental study of performance of geogrid-reinforced retaining wall subjected to load from strip foundation at top surface of wall. *Rock Soil Mech.* **2013**, *34*, 1586–1592.
29. Li, S.; Cai, X.; Jing, L.; Xu, H.; Zhu, C. Reinforcement strain and potential failure surface of geogrid reinforced soil-retaining wall under horizontal seismic loading. *Shock. Vib.* **2020**, *2020*, 1–17. [[CrossRef](#)]
30. Ausilio, E.; Conte, E.; Dente, G. Seismic stability analysis of reinforced slopes. *Soil Dyn. Earthq. Eng.* **2000**, *19*, 159–172. [[CrossRef](#)]
31. Richards, R.; Dims, D.G. Seismic behavior of gravity retaining walls. *J. Geotech. Eng. ASCE* **1979**, *105*, 449–464.
32. Whitman, R.V.; Liao, S. *Seismic Design of Gravity Retaining Walls*; WCEE: San Francisco, CA, USA, 1985; pp. 533–540.
33. Newmark, N.M. Effect of earthquakes on dams and embankments. *Geotechnique* **1965**, *15*, 139–159. [[CrossRef](#)]
34. Huang, C.C.; Chou, L.H.; Tatsuoka, F. Seismic displacements of geosynthetic-reinforced soil modular block walls. *Geosynth. Int.* **2003**, *10*, 2–23. [[CrossRef](#)]